Temperature-dependent magnetic properties of ferrimagnetic $DyCo_3$ alloy films

Kai Chen,[1,*] Dieter Lott,[2] Florin Radu,[3] Fadi Choueikani,[1] Edwige Otero,[1] and Philippe Ohresser[1]
[1]*Synchrotron SOLEIL, L'Orme des Merisiers, Saint-Aubin-BP48, 91192 Gif-sur-Yvette CEDEX, France*
[2]*Institute for Materials Research, Helmholtz-Zentrum Geesthacht, 21502 Geesthacht, Germany*
[3]*Helmholtz-Zentrum Berlin für Materialien und Energie, Albert-Einstein-Straße 15, 12489 Berlin, Germany*
(Received 9 October 2014; revised manuscript received 17 December 2014; published 9 January 2015)

Synchrotron soft x-ray magnetic circular and linear dichroism (XMCD and XMLD) spectroscopies at the Dy $M_{4,5}$ and Co $L_{2,3}$ edges are reported to investigate the temperature-dependent magnetic properties of rare earth–transition metal $DyCo_3$ alloy films. In a temperature region between 4.4 K and 300 K, the two sites of Co and Dy are ferrimagnetic alloy coupled, with the Dy magnetization aligned to the applied field as the dominant site. The combined method of XMCD and XMLD and the application of the sum rules allows one to monitor the detailed changes in the magnetic contribution from both sites separately. It reveals that Dy possesses a very large moment of 8.2 μ_B/atom at low temperatures. At higher temperatures, the reduction of the total magnetic moment is dominated by the behavior of the Dy magnetic moments which exhibit a steeper decrease, especially in the temperature regime between 150 K and 200 K. The reoccupation of the Zeeman split levels of the $4f$ sites of Dy indicates that thermal fluctuations are the driving force.

DOI: 10.1103/PhysRevB.91.024409 PACS number(s): 75.47.Np, 75.50.Gg, 75.50.Kj, 75.70.−i

I. INTRODUCTION

The rich magnetic phases and the straightforward way to control their magnetic properties have made amorphous alloys consisting of rare earth (RE) and $3d$ transition metal (α-RE-TM alloys) extremely interesting for applied as well as fundamental studies of magnetism. Particularly, alloys with heavy RE sites such as Gd, Dy, or Tb have been investigated since the 1980s and considered as extremely promising candidates for perpendicular recording media due to their inherent perpendicular anisotropy in thin films [1,2]. Recently, α-RE-TM alloys were further utilized in magnetic hybrid structures exhibiting strong exchange bias (EB) effects [3–6]. Here, the ferrimagnetic (FI) nature of α-RE-TM alloys with heavier RE elements was used to replace the hard antiferromagnetic (AF) layer [5] as well as even the soft magnetic ferromagnetic (FM) component [6] in EB systems enabling one to construct an EB mechanism where the switching of the sign of the EB field can be governed by the application of low magnetic fields avoiding the laborious field-cooling procedure which is necessary in conventional exchange bias systems using AF/FM components. Another intriguing experiment was carried out to study ultrafast dynamic switching phenomena in α-RE-TM alloys [7]. It was shown that under certain conditions the combination with a TM site significantly enhances the switching time of the RE component, which may be extremely important with respect to the use of RE sites for future spintronics devices.

Even though the fascinating nature of these α-RE-TM alloys has been extensively studied and used for decades, the precise coupling mechanism between both magnetic sites as well as the origin of the inherent anisotropy in these amorphous systems are still not completely understood. Detailed band structure calculations could demonstrate that the polarization of the $5d$ bands overlapping with the strongly localized $4f$ states in the RE site is one of the keys to explain how the itinerant magnetism of the RE sites is coupled so strongly with band magnetism of the TM sites [8]. In heavier RE, the antiferromagnetic polarization of the $5d$ bands with respect to the $4f$ band results in an antiferromagnetic coupling between the RE and TM leading to the ferrimagnetic nature of many α-RE-TM alloys. While at low temperature the magnetic moment of the RE site is in general dominating, the magnetic moment of the TM site becomes finally larger above the compensation temperature, at which both magnetic contributions cancel out, reducing the overall moment of the alloy to zero. The compensation temperature of such α-RE-TM alloys may be tuned by changing the ratio of constituent elements [9].

For the investigation of the coupling behavior between these two magnetic sites an investigation tool is needed which allows one to probe the different magnetic contributions of the system in a very detailed way. The element-specific x-ray magnetic circular (XMCD) and linear dichroism (XMLD) are ideal techniques, particularly for the investigation of such amorphous systems consisting of two magnetic constituents. They allow one to probe the magnetism of both sites separately by tuning the x-ray energy to the particular absorption edges, thus being only sensitive to one specific magnetic site at a time. In this paper we study the magnetic behavior of α-RE-TM alloys consisting of Dy as the RE and Co as the TM component in a composition ratio of about one to three which will be denoted here as $DyCo_3$. At this ratio, the Dy site dominates the magnetic contributions in the alloy far above room temperature [10]. However, strong changes in the total magnetic moment as well as in the anisotropy of the system are expected already below 300 K due to different temperature dependence of magnetic order parameters between the Dy and Co sites. In the following we present the results of detailed temperature-dependent XMCD and XMLD measurements from 4.4 to 300 K, and discuss the temperature dependence of the magnetic behavior of $DyCo_3$ by applying the sum rules.

II. SAMPLES AND EXPERIMENTAL SETUP

$DyCo_3$ samples were prepared by magnetron sputtering (MAGSSY chamber at BESSY) in an ultraclean argon atmosphere of 1.5×10^{-3} mbar with a base pressure of

*Corresponding author: kai.chen@synchrotron-soleil.fr

$p < 5 \times 10^{-9}$ mbar at the deposition temperature of 300 K. The stoichiometry of the ferrimagnetic alloys was controlled by varying the deposition rate of separate chemical elements in a co-evaporation scheme. Si_3N_4 membranes with a surface area of 5×5 mm^2 and a thickness of 100 nm were used as substrates for the soft x-ray transmission measurements. A capping layer of 3 nm of tantalum (Ta) was grown on the 50 nm thick $DyCo_3$ layer to prevent surface oxidation.

X-ray absorption (XAS), XMCD, and XMLD spectra at the Co $L_{2,3}$ and Dy $M_{4,5}$ edges were measured at temperatures from 4.4 K to 300 K in transmission geometry at synchrotron-SOLEIL using the 7T cryomagnet installed on the DEIMOS (Dichroism Experimental Installation for Magneto-Optical Spectroscopy) beamline [11]. The XMCD studies were carried out using x rays of circular right (CR) and left (CL) polarizations with a magnetic field of $\mu_0 H = 7$ T applied along the x-ray beam, while the XMLD was measured with linear polarized (with $E//H$ or $E \perp H$) x rays with a magnetic field of $\mu_0 H = 2$ T applied along the sample (perpendicular to the beam). For the magnetic sensitivity to the individual magnetic elements, the characteristic energies for the Co $L_{2,3}$ and the Dy $M_{4,5}$ edges were selected. The XMCD and XMLD data were recorded as $(\sigma^+ - \sigma^-)$ and $(\sigma_\perp - \sigma_{//})$, respectively, where σ^+ and σ^- denote the absorption cross section for right and left circular polarized x rays and $\sigma_\perp$ and $\sigma_{//}$ the absorption cross section for linear polarized x rays with an external magnetic field applied perpendicular (LV) and parallel (LH) to the propagation direction of the x rays. The magnetic hysteresis measurements were performed by taking the difference of $(\sigma^+ - \sigma^-)$ with the photon energy for the x-ray beam set to the value at the L_3 edge of Co or M_5 edge of Dy where the XMCD signal is maximized. As using transmission measurements [24] the experimental XMCD and XMLD were extracted as the logarithm of the ratio of the transmitted x-ray intensities of different polarization states (CR and CL) or for orthogonal magnetic field orientations, respectively.

III. EXPERIMENTAL RESULTS

A. Result of XAS and XMCD measurements

Figure 1 shows the XAS and XMCD spectra measured at the Co $L_{2,3}$ and Dy $M_{4,5}$ edges at the two temperatures of 4.4 K and 300 K. At both temperatures strong XMCD signals for both elements, Co and Dy, are observed. With the temperature increasing from 4.4 K to 300 K, the XMCD signal for Co exhibits a small reduction in magnitude of only about 10% but no significant changes in the line shape indicating that for this temperature range the magnetic properties for Co remain nearly unchanged. In the case of Dy the XMCD signal undergoes a considerable change with temperature, as revealed by the occupation of the Zeeman split $4f$ states, denoted as M_J

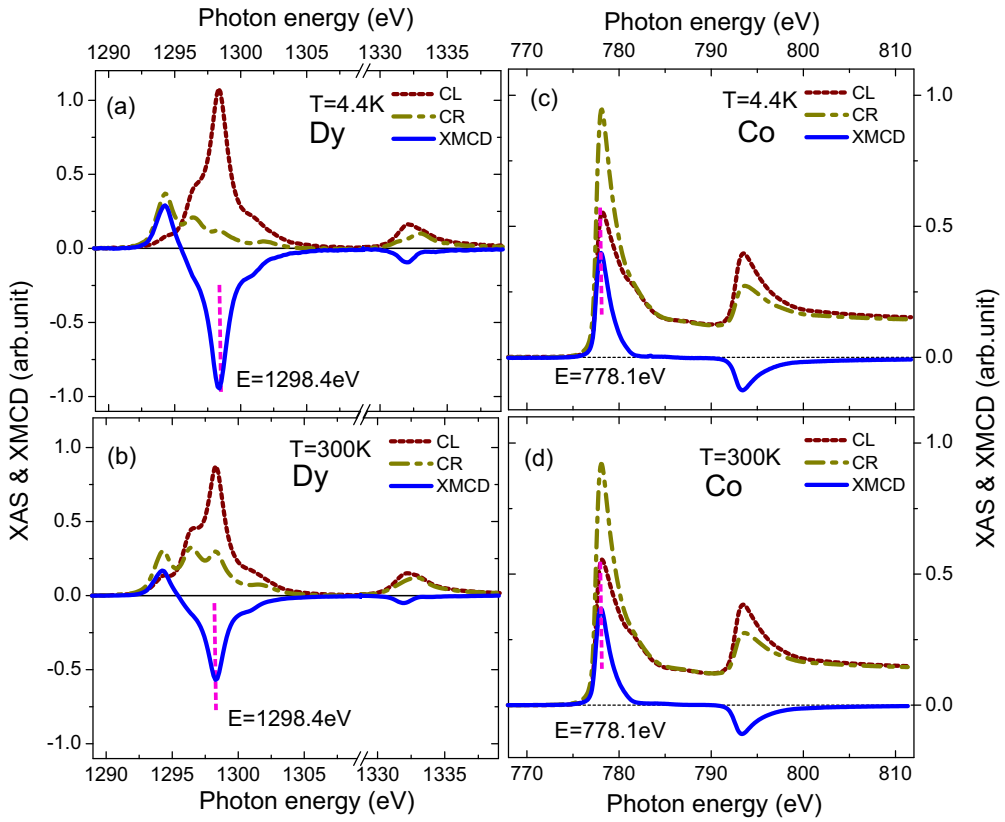

FIG. 1. (Color online) XAS and XMCD spectra with the magnetic field applied normal to the film plane for Dy $M_{4,5}$ edges at 4.4 K (a) and 300 K (b) and Co $L_{2,3}$ at 4.4 K (c) and 300 K (d). For both temperatures, the negative XMCD signal at Dy $M_{4,5}$ edges indicates that the magnetization of Dy is parallel while the positive XMCD signal at Co L_3 indicates the magnetization of Co is antiparallel to the external field, resulting in a ferrimagnetic coupling in the alloy. The photon energies of Dy M_5 and Co L_3 which are used for the magnetic hysteresis measurements are marked in the figures.

states. The origin of the dichroism for RE in general and for Dy in particular resides in the unequal occupation of the M_J states, which follows the Boltzmann distribution and is determined by the competition between Zeeman splitting energy $\mu_B g H$ and thermal fluctuation $k_B T$ [12]. At a low temperature of 4.4 K where the thermal energy is significantly smaller than the magnetic splitting, the lower-lying Zeeman level $M_J = -15/2$ has higher priority to be occupied while at 300 K there exist more occupied higher-lying $M_J \neq -15/2$ states, resulting in the change of the XAS line shape as observed here. This reshuffle of the different substates is accompanied with a strong decrease of the magnetic moment at the Dy site as can be clearly seen in the reduction of the XMCD signal at $T = 300$ K [see Fig. 1(b)]. At even higher temperatures all the states (from $-15/2$, $-13/2, \ldots,$ to $15/2$) are occupied randomly and the XMCD signal will eventually disappear. One should note that the XMCD signals ($\sigma^+ - \sigma^-$) for Co and Dy have different signs at both temperatures, showing their antiparallel alignment with the dominant Dy moments aligned parallel to the applied magnetic field at 4.4 K and 300 K. As already pointed out above, the $DyCo_3$ alloy is a ferrimagnet with its compensation temperature above room temperature ($T_{comp} \approx 380$ K), which is reasonable since the T_{comp} for $DyCo_5$ and $DyCo_{3.35}$ are around 120 K [6] and 300 K [9,13], respectively, and thus no change of the magnetic dominant site is expected, even at room temperature.

The temperature dependence of the absorption spectra for the left and right circularly polarized x rays as well as for the resulting XMCD signal at the Dy M_5 edge are shown in Fig. 2. Here one should notice that the changes in the behavior are most dominant in a temperature range from 150 K to 200 K where the temperature-dependent occupation of the higher Zeeman splitting M_J states is particularly enhanced. The XMCD signal decreases most drastically from 150 K to 200 K while for lower and higher temperatures the changes are more moderate.

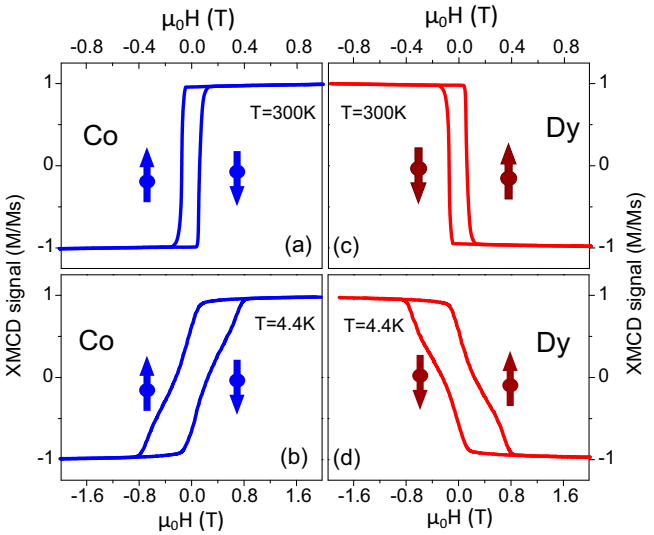

FIG. 3. (Color online) Hysteresis measured at Co L_3 edge and Dy M_5 edge with the magnetic field applied out-of-plane and the temperature of 300 K [(a), (c)] and 4.4 K [(b), (d)].

To investigate the macroscopic behavior of magnetization in more detail between both elements, element-specific magnetic hysteresis curves were recorded by measuring the field-dependent XMCD signal at the Co L_3 edge and the Dy M_5 edge. The photon energy is selected at the maximum of the XMCD signal, meaning at 778.1 eV and 1298.4 eV, respectively. Figure 3 shows the element-specific hysteresis curves for Co and Dy at 300 K and 4.4 K. The magnetic field sweeps are carried out with the magnetic field aligned in the out-of-plane

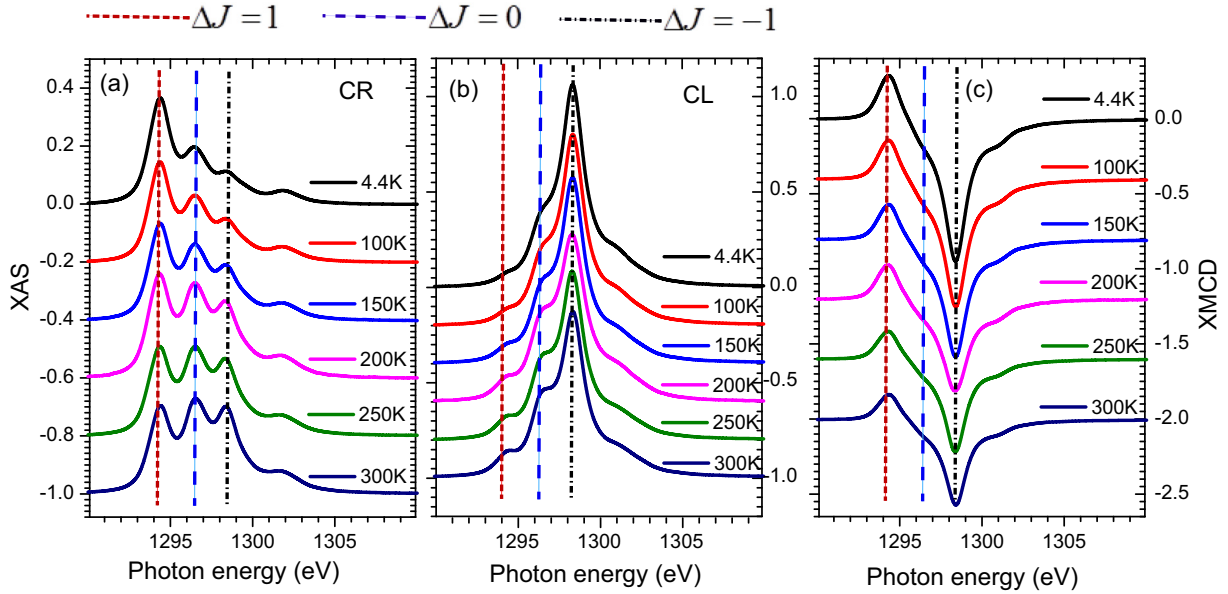

FIG. 2. (Color online) The temperature-dependent XAS [(a) and (b) for σ^+ (CR) and σ^- (CL), respectively] and (c) XMCD ($\sigma^+ - \sigma^-$) of Dy M_5 edge from 4 to 300 K. The peaks marked in the panels at $E = 1294.3$, 1296.5, and 1298.4 eV are from the excitation with $\Delta J = +1, 0, -1$. With the temperature increasing, the XMCD signal is decreasing with a reduced magnetic moment. Besides, the shape of the XAS (both for σ^+ and σ^-) is changing indicating the change of the occupation of the Zeeman splitting ground state of the $4f$ electrons in Dy.

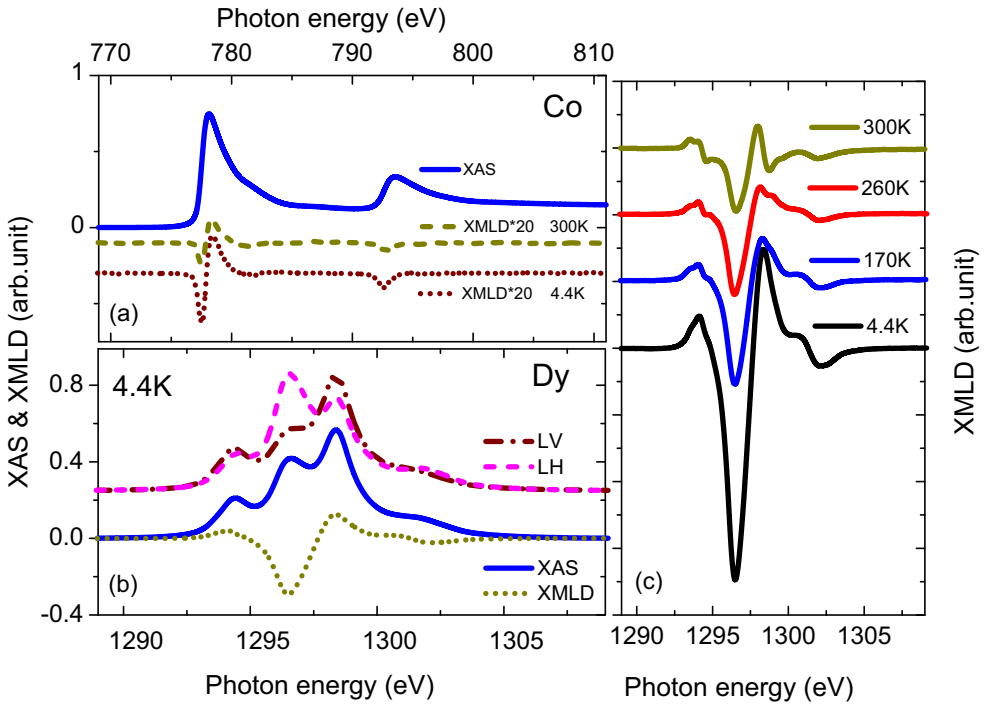

FIG. 4. (Color online) (a) XAS and XMLD at Co $L_{2,3}$ edges and at temperature of 4.4 K and 300 K. (b) XAS of Dy M_5 edge using x rays with different linear polarizations of linear horizontal ($\sigma_{//}$), linear vertical ($\sigma_{\perp}$), and the XMLD spectra of $\sigma_{\mathrm{XMLD}} = \sigma_{//} - \sigma_{\perp}$ at 4.4 K; for comparison isotropic XAS (solid curve) of absolute cross section $\sigma_0 = (\sigma_{//} + 2\sigma_{\perp})/3$ is also shown which remains the same at different temperatures. (c) XMLD of Dy at different temperatures from 4.4 K to 300 K.

direction. As depicted at 4.4 K and 300 K in Fig. 3, Co and Dy exhibit mirrored hysteresis curves demonstrating their strict antiferromagnetic coupling in this ferrimagnetic alloy which is also present for all other measured temperatures (not shown here). At 300 K the out-of-plane hysteresis curves show a very squared loop behavior with the remanent magnetization (M_R) quasiequal to the saturation magnetization (M_S), indicating a remanent single domain spin structure in the film. At low temperature (LT) of 4.4 K, the shapes of the curves are drastically different. A strongly tilted hysteresis loop with a reduced M_R compared to M_S is observed, which indicates the formation of a remanent multidomain spin structure in the film. For magnetic systems with an out-of-plane anisotropy, as is expected for $DyCo_3$, the formation of magnetic domains is due to the competition between the perpendicular anisotropy and the demagnetization. At RT the perpendicular magnetic anisotropy is dominating while at LT the strong demagnetization fields created by the increased value of the macroscopic magnetization fields lead to a multidomain state.

B. Result of XMLD measurements

In order to fully understand the magnetic behavior in such alloys containing RE elements with its large spin-orbit coupling, it must be noticed that not all contributions of the magnetic moments can be extracted solely by the XMCD data. Linear effects containing information about the magnetic anisotropy due to spin-orbit coupling effects play here an important role. Therefore, measurement of the XMLD signal are required to collect this additional and necessary information, i.e., being able to derive the magnetic moment for each element by applying the sum rules as will be explained in more detail in the theoretical discussion section.

Figure 4 shows the XMLD data measured at the Co $L_{2,3}$ and Dy M_5 edges, at 4.4 K and 300 K. The XMLD signal of Co ($\times 20$ for a better visibility) is very weak (3%) and thus similar to the signal of bulk Co [14–17]. With the temperature increasing from 4.4 K to 300 K, the faint XMLD signal is even more reduced by almost 30%. In comparison to the corresponding XMCD signal the XMLD signal is more than 30 times smaller. For Dy, on the other hand, the XMLD intensities are very strong at both temperatures. Figure 4(b) shows the spectra at 4.4 K for the two linear polarization states of the x rays, LH and LV, marked as $\sigma_{//}$ and $\sigma_{\perp}$, the isotropic XAS $\sigma_0 = (\sigma_{//} + 2\sigma_{\perp})/3$, and the XMLD ($\sigma_{\perp} - \sigma_{//}$) signal. The main contribution stems from changes in the $\Delta J = 0$ state as it is in general expected for XMLD reaching nearly the same magnitude as the average XAS signal. In Fig. 4(c) the XMLD signal is plotted for different temperatures showing its reduction with increasing temperature. According to theory, the XMLD data follow the same thermal variation as the XMCD signal which can be understood since circular and linear polarization are built with the similar temperature-dependent $\langle J_z \rangle$ and $\langle J_z^2 \rangle$ terms [see Eqs. (5) and (6) below]. At 300 K, the XMLD signal of Dy is only 20% of that at 4.4 K, while the isotropic XAS of σ_0 remains constant.

IV. THEORETICAL DISCUSSION

Since 1985 strong magnetic dichroism has been theoretically predicted in the $M_{4,5}$ x-ray absorption spectra of

rare-earth materials [18] and later confirmed by experiments [19,20]. Based on the local multiplet calculation, Schille *et al.* developed the formula for the absorption cross section as a function of the polarization of the light [21], which is

$$\sigma(\omega) = \sigma_0(\omega) + i(\epsilon \times \epsilon^*)\langle J\rangle\sigma_1(\omega) + \left(\frac{\langle(\epsilon\cdot J)(\epsilon^*\cdot J)+(\epsilon^*\cdot J)(\epsilon\cdot J)\rangle}{2} - \frac{J(J+1)}{3}\right) \times \sigma_2(\omega), \quad (1)$$

$$\sigma^+(\omega) = \sigma_0(\omega)+\langle J_z\rangle\sigma_1(\omega) + \frac{1}{2}\left(\frac{J(J+1)}{3} - \langle J_z^2\rangle\right)\sigma_2(\omega), \quad (2)$$

$$\sigma^-(\omega) = \sigma_0(\omega) - \langle J_z\rangle\sigma_1(\omega) + \frac{1}{2}\left(\frac{J(J+1)}{3} - \langle J_z^2\rangle\right)\sigma_2(\omega), \quad (3)$$

$$\sigma_{//}(\omega) = \sigma_0(\omega) + \left(\langle J_z^2\rangle - \frac{J(J+1)}{3}\right)\sigma_2(\omega), \quad (4)$$

$$\sigma_{\mathrm{XMCD}}(\omega) = 2\langle J_z\rangle\sigma_1(\omega), \quad (5)$$

$$\sigma_{\mathrm{XMLD}}(\omega) = \frac{1}{2}\left[3\langle J_z^2\rangle - J(J+1)\right]\sigma_2(\omega). \quad (6)$$

According to the Eqs. (1)–(6), it is essential to consider the term $\sigma_0 = (\sigma^+ + \sigma^- + \sigma_{//})/3$, where $(\sigma^+ + \sigma^-)/2$ is equal to $\sigma_\perp$, to calculate the magnetic moment of rare-earth materials with the help of sum rules. Due to the strong spin-orbit splitting in rare-earth elements, the assumption of $\sigma_\perp = \sigma_{//}$ which is often used successfully to calculate the sum rules in $3d$ transition metals with its weak orbital moments is no longer valid. Using this approximation would cause a significant additional error of up to 10% for low temperatures due to the strong XMLD effect in rare-earth materials.

In Fig. 5 the experimental results of σ^+, σ^-, $\sigma_{//}$, σ_0, XMCD, and XMLD measured at 4.4 K are compared to the theoretical calculations assuming Dy^{3+} in its pure $J = -\frac{15}{2}$ ground state from [12,20] by applying Eqs. (1)–(6). The experimental spectra [Fig. 5(b)] agree here qualitatively well with the theoretical calculations [Fig. 5(a)]; however, it is clearly shown that even at temperatures as low as 4.4 K and in an applied magnetic field of 6 T, some higher-lying Zeeman states of $M_J \neq -15/2$ in Dy are already occupied due to thermal fluctuations. Moreover, the magnitudes of the experimental signal are significantly lower and need to be scaled. By keeping the same shape, the experimental XMCD signal and the XMLD signal are about 75% and 30% compared to the signal calculated by theory. As already pointed out, the presence of thermal fluctuations justifies that also higher M_J levels are occupied even at low temperatures. According to theory, with $M_J = -15/2$ the state of $\Delta J = -1$, $\Delta J = 0$, or $\Delta J = +1$ can only be excited by x rays with polarization of CL, LH, or CR, respectively. For the states $M_J \neq -15/2$, the x-ray absorption spectra with polarization of CL, LH, or CR are mixed with the spectra of $\Delta J = -1$, $\Delta J = 0$, and $\Delta J = +1$. In order to model the experimental data, the different levels are adjusted independently to estimate their contribution to the different spectra. In Fig. 5(c) the theoretical spectra of $\Delta J = -1,0,+1$ are mixed accordingly to fit the experimentally measured spectra σ^- (CL) leading to a certain contribution of the mixed states as $\Delta J = +1$ (5%), $\Delta J = 0$ (21%), and $\Delta J = -1$ (74%); and $\Delta J = +1$ (74%), $\Delta J = 0$ (21%), and $\Delta J = -1$ (5%) for the spectra σ^+ (CR). For the spectra $\sigma_{//}$ (LH), it is mixed with $\Delta J = +1$ (23%), $\Delta J = 0$ (54%), and $\Delta J = -1$ (23%) with the equal contributions from $\Delta J = +1$ and $\Delta J = -1$ states. At $T = 300$ K, the higher M_J states are even more occupied leading to stronger changes in the shape of the spectra, which, on the other hand, has a consequence that the XMCD and XMLD signal are drastically reduced. It should be noted that the isotropic spectra of σ_0 is independent of M_J and of the temperature, keeping the same shape and magnitude for all temperatures from 4.4 K to 300 K.

By applying the sum rules [22–24] it is possible to determine the effective spin magnetic moment m_S^{eff} and the orbital magnetic moment m_L:

$$\frac{\int_{\mathrm{edge}} dw(\mu^+ - \mu^-)}{\int_{\mathrm{edge}} dw(\mu^+ + \mu^- + \mu_{//})} = \frac{1}{2}\frac{c(c+1) - l(l+1) - 2}{l(l+1)(4l+2-n)}M_L, \quad (7)$$

$$\frac{\int_{j_+} dw(\mu^+ - \mu^-) - [(c+1)/c]\int_{j_-} dw(\mu^+ - \mu^-)}{\int_{j_+ + j_-} dw(\mu^+ + \mu^- + \mu_{//})} = \frac{1}{2}\frac{l(l+1) - c(c+1) - 2}{3c(4l+2-n)}M_S^{\mathrm{eff}}. \quad (8)$$

For Co $L_{2,3}$ we have $c = 1$ and $l = 2$ while for Dy $M_{4,5}$ we have $c = 2$ and $l = 3$. Here, n or $(4l + 2 - n)$ are the numbers of electrons or holes in Co $3d$ and Dy $4f$ states, respectively. The effective spin moment $M_s^{\mathrm{eff}} = M_S + C \cdot m_T$ ($C = 7$ for Co and 6 for Dy) consists of the spin magnetic moment m_s and the magnetic dipole moment m_t which accounts for the asphericity of the spin moment distribution. Figure 6 shows the temperature-dependent magnetic spin M_S (μ_B/hole), orbital M_L (μ_B/hole), and total moments M_{total} (μ_B/atom) of Dy and Co, from 4.4 K to 300 K. Since the magnetic dipole operator is weak in TM bulk materials with weak spin-orbital coupling, its contribution is neglected.

The spin moment of Co slightly decrease from 0.60 to 0.53 μ_B/hole (10% reduced) from 4.4 K to 300 K, while the weak orbital moment is slightly lower in the temperature range from 150 K to 200 K. If we take $n = 2.49$ as the number of holes in Co, as averaged from those values reported in theoretical calculations [25–27], the total magnetic moment can be calculated as shown in Fig. 6(c). It follows the tendency of M_S since the orbital contribution is extremely small compared to the spin moment. The maximum magnetic moment of Co is 1.66 μ_B/atom observed at 4.4 K which is 6% smaller compared to 1.77 μ_B/atom for bulk Co [24].

The strong spin-orbital coupling in a $4f$ element such as Dy does not allow us to simply neglect the contribution of the magnetic dipole operator. On the basis of an atomic model, the expected value of the magnetic dipole operator was estimated to be -0.128 μ_B/atom [31] or -0.0256 μ_B/hole due to the $4f^9$ ground state configuration ($n = 5$) of Dy. Under this assumption the magnetic moments of M_S, M_L, and M_{total} for Dy can be calculated as shown in Figs. 6(d)–6(f). All

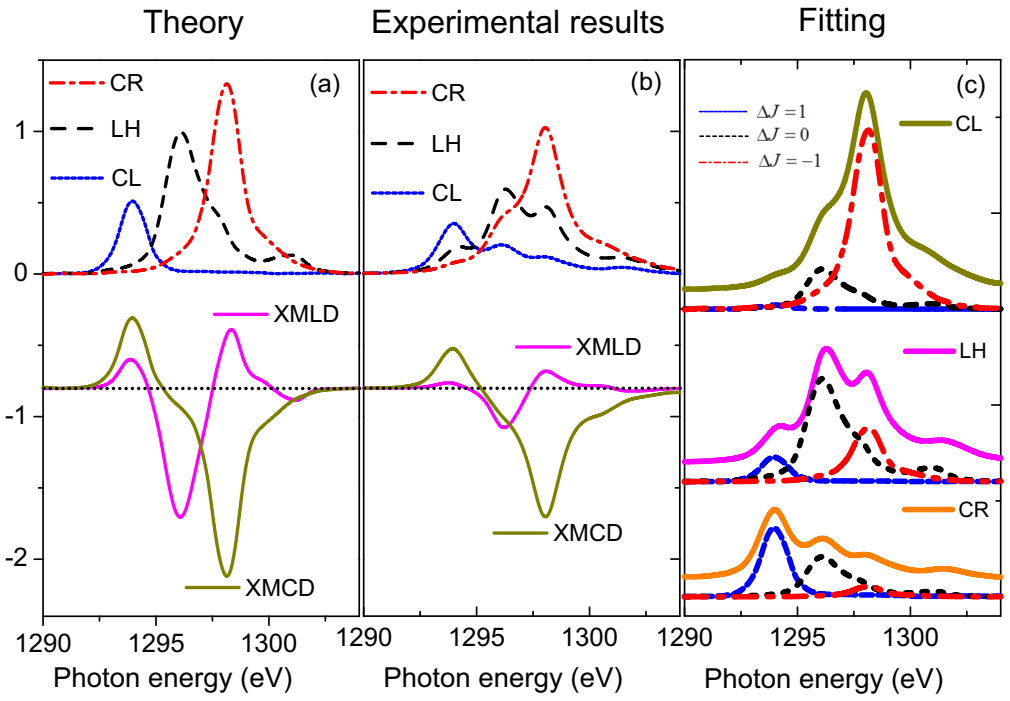

FIG. 5. (Color online) Results of σ^+ (CR), σ^- (CL), $\sigma_{//}$ (LH), XMCD, and XMLD measured at 4.4 K (b) are compared to the theoretical calculations (a) of Dy^{3+} in its $J = -15/2$ ground state [12,20]. (c) Fitting of the experimental results with the theoretical spectra of $\Delta J = +1,0,-1$.

three values decrease steadily with increasing temperature; however, between 150 and 200 K, the decay is particularly strong, while in the regimes from 4.4 K to 150 K and 200 K to 300 K the reduction of the moments is quite moderate. It should be pointed out that for $DyCo_3$ at 4.4 K, the magnetic moment of Dy is about 8.2 μ_B/atom, which is 82% of the theoretical results of 10 μ_B. This value is much higher if compared to other Dy-based materials, such as $Dy@C_{82}$ [28],

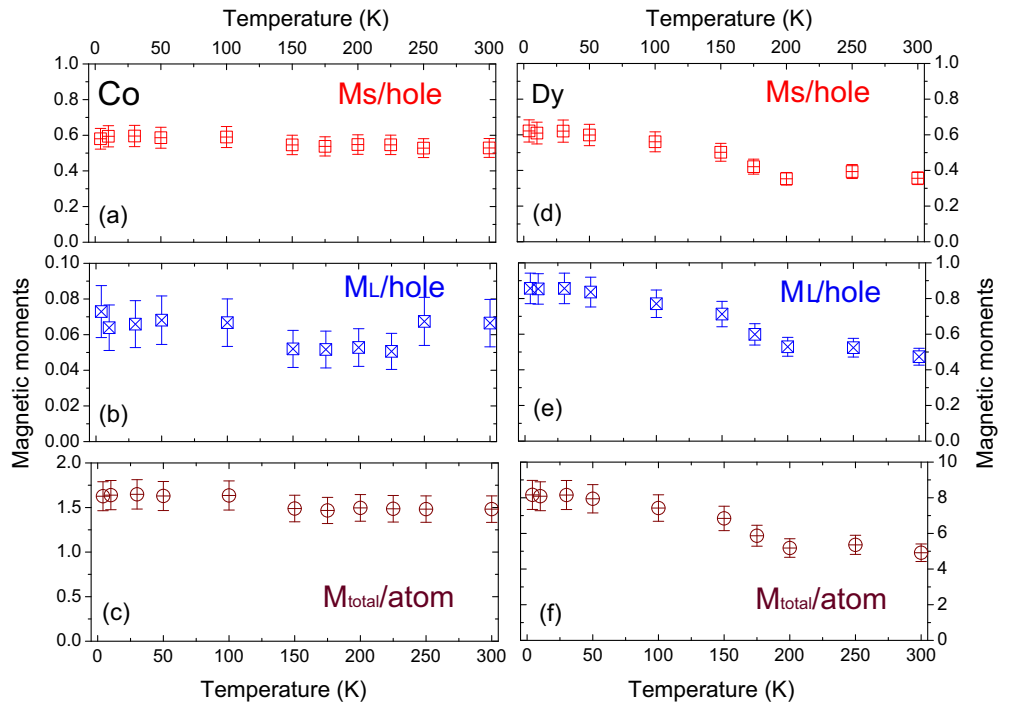

FIG. 6. (Color online) The temperature-dependent magnetic spin M_S (μ_B/hole), orbital M_L (μ_B/hole), and total moments M_{total} (μ_B/atom) of Dy and Co, from 4.4 K to 300 K; error bars of each points are also shown (20% for M_L of Co and 10% for the rest). Rapid decreasing of the magnetization has been observed at around 180 K for both elements.

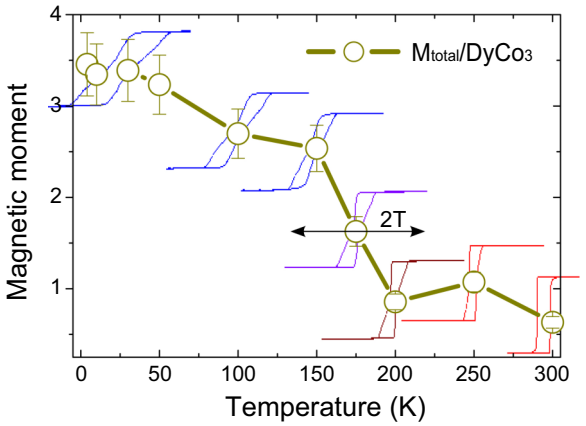

FIG. 7. (Color online) The temperature-dependent magnetization M_{total} (μ_B/$DyCo_3$), as well as the magnetic hysteresis loops at Dy M_5 edge. With the temperature increasing, the out-of-plane anisotropy appears and the saturation magnetization drops rapidly above 150 K.

$DySc_2N@C_{80}$ [29], Dy incar-fullerenes [30,32], and DyN [33], where the magnetic moment is almost 50% or even more reduced at the low temperature of 4.4 K. One strong indication of the reduced magnetic moment of these systems at such low temperatures is the more occupied higher $M_J \neq -15/2$ state that resembles the shape to that observed for $DyCo_3$ at 300 K. Conversely, one can speculate that the strong ferrimagnetic coupling between Dy and Co in $DyCo_3$ favors the higher occupation of lower-lying Zeeman splitting M_J states which results in a high magnetic moment in Dy for this compound.

The net magnetization of the ferrimagnetically coupled $DyCo_3$ can be calculated in a straightforward way by $M_{\text{total}} = M_{\text{Dy}} - 3M_{\text{Co}}$ by combining the values of the individual moments derived above. Figure 7 shows the temperature-dependent magnetization M_{total} measured at a magnetic field of $\mu_0 H = 6$ T in the out-of-plane direction, together with the corresponding magnetic hysteresis loops measured at the Dy M_5 edge. The behavior of the total magnetization is mainly determined by the magnetic behavior of the Dy site as discussed above. Particularly, a strong decay of the total magnetization is observed between 150 K and 200 K leading to strong changes in the shape of the hysteresis loop. The competition between the perpendicular anisotropy and the demagnetization fields is very strong, as already discussed earlier for Fig. 3. Below and above this temperature region one of these forces becomes more dominant being responsible for the multidomain state at low temperatures or single-domain state at higher temperatures.

V. CONCLUSION

In conclusion, by means of XMCD and XMLD soft x-ray spectroscopic techniques we have studied the temperature dependence of the elemental magnetic moments of $DyCo_3$ films with perpendicular anisotropy. The elemental magnetic moments of Co exhibit a slower evolution as a function of temperature, whereas the Dy moments show a larger change as a function of temperature. A very high magnetic moment for Dy of 8.2 μ_B/atom was observed at 4.4 K which is only 20% less than the theoretical value and much higher compared to any other experimental results of Dy compounds reported so far. Moreover we show clearly that the reduction of the Dy moment and thus the total moment of the antiferromagnetically coupled $DyCo_3$ occurs mainly in a temperature range between 150 K and 200 K, supported also by an indicative change of the magnetic hysteresis loop shape. At this transition the XAS spectra taken with linear and circular polarized light also show a very strong redistribution of the M_J states which can be understood by the influence of thermal fluctuation on the occupation level of the Zeeman split 4*f* states. It should be pointed out that these changes are far from the T_{comp} of the alloy and are not associated with the change of the dominant magnetic site. These results are very helpful for a more profound understanding of the fundamental properties of such amorphous RE-TM alloys which are used in many magnetic hybrid structures nowadays, showing intriguing magnetic properties and a great potential for future applications.

ACKNOWLEDGMENTS

We acknowledge Synchrotron-Soleil for provision of synchrotron radiation facilities.

[1] M. Mansuripur and M. F. Ruane, IEEE Trans. Magn. **22**, 33 (1986).
[2] S. V. Eliseeva and J.-C. G. Bunzli, New J. Chem. **35**, 1165 (2011).
[3] F. Hellman, R. B. van Dover, and E. M. Gyorgy, Appl. Phys. Lett. **50**, 296 (1987).
[4] W. C. Cain and M. H. Kryder, J. Appl. Phys. **67**, 5722 (1990).
[5] C. Schubert, B. Hebler, H. Schletter, A. Liebig, M. Daniel, R. Abrudan, F. Radu, and M. Albrecht, Phys. Rev. B **87**, 054415 (2013).
[6] F. Radu, R. Abrudan, I. Radu, D. Schmitz, and H. Zabel, Nat. Commun. **3**, 715 (2012).
[7] V. López-Flores, N. Bergeard, V. Halt, C. Stamm, N. Pontius, M. Hehn, E. Otero, E. Beaurepaire, and C. Boeglin, Phys. Rev. B **87**, 214412 (2013).
[8] E. Burzo and L. Chioncel, J. Optoelectron. Adv. Mater. **6**, 917 (2004).
[9] A. Aguia, M. Mizumaki, T. Asahi, K. Matsumoto, T. Morikawa, J. Sayama, and T. Osaka, J. Phys. Chem. Solids **68**, 2148 (2007).
[10] J. K. Yakinthos and D. E. Mentzafos, Phys. Rev. B **12**, 1928 (1975).
[11] P. Ohresser, E. Otero, F. Choueikani, K. Chen, S. Stanescu, F. Deschamps, T. Moreno, F. Polack, B. Lagarde, J.-P. Daguerre, F. Marteau, F. Scheurer, L. Joly, J.-P. Kappler, B. Muller, O. Bunau, and Ph. Sainctavit, Rev. Sci. Instrum. **85**, 013106 (2014).
[12] J. B. Goedkoop, B. T. Thole, G. van der Laan, G. A. Sawatzky, F. M. F. de Groot, and J. C. Fuggle, Phys. Rev. B **37**, 2086 (1988).
[13] A. Agui, M. Mizumaki, T. Asahi, J. Sayama, K. Matsumoto, T. Morikawa, T. Matsushita, T. Osaka, and Y. Miura, J. Alloys Compd. **408-412**, 741 (2006).

[14] M. M. Schwickert, G. Y. Guo, M. A. Tomaz, W. L. O'Brien, and G. R. Harp, Phys. Rev. B **58**, R4289 (1998).
[15] S. S. Dhesi, G. van der Laan, and E. Dudzik, Appl. Phys. Lett. **80**, 1613 (2002).
[16] W. Kuch, F. Offi, L. I. Chelaru, J. Wang, K. Fukumoto, M. Kotsugi, J. Kirschner, and J. Kunes, Phys. Rev. B **75**, 224406 (2007).
[17] J. Kuneš, P. M. Oppeneer, S. Valencia, D. Abramsohn, H.-Ch. Mertins, W. Gudat, M. Hecker, and C. M. Schneider, J. Magn. Magn. Mater. **272-276**, 2146 (2004).
[18] B. T. Thole, G. van der Laan, and G. A. Sawatzky, Phys. Rev. Lett. **55**, 2086 (1985).
[19] M. Sacchi, O. Sakho, and G. Rossi, Phys. Rev. B **43**, 1276 (1991).
[20] R. J. H. Kappert, J. Vogel, M. Sacchi, and J. C. Fuggle, Phys. Rev. B **48**, 2711 (1993).
[21] J. Ph. Schille, J. P. Kappler, Ph. Sainctavit, Ch. Cartier dit Moulin, C. Brouder, and G. Krill, Phys. Rev. B **48**, 9491 (1993).
[22] B. T. Thole, P. Carra, F. Sette, and G. van der Laan, Phys. Rev. Lett. **68**, 1943 (1992).
[23] P. Carra, B. T. Thole, M. Altarelli, and X. Wang, Phys. Rev. Lett. **70**, 694 (1993).
[24] C. T. Chen, Y. U. Idzerda, H.-J. Lin, N. V. Smith, G. Meigs, E. Chaban, G. H. Ho, E. Pellegrin, and F. Sette, Phys. Rev. Lett. **75**, 152 (1995).
[25] G. Y. Guo, H. Ebert, W. M. Temmerman, and P. J. Durham, Phys. Rev. B **50**, 3861 (1994).
[26] R. Wu, D. Wang, and A. J. Freeman, Phys. Rev. Lett. **71**, 3581 (1993).
[27] R. Wu and A. J. Freeman, Phys. Rev. Lett. **73**, 1994 (1994).
[28] R. Kitaura, H. Okimoto, H. Shinohara, T. Nakamura, and H. Osawa, Phys. Rev. B **76**, 172409 (2007).
[29] R. Westerström, J. Dreiser, C. Piamonteze, M. Muntwiler, S. Weyeneth, H. Brune, S. Rusponi, F. Nolting, A. Popov, S. Yang, L. Dunsch, and T. Greber, J. Am. Chem. Soc. **134**, 9840 (2012).
[30] C. De Nadaï, A. Mirone, S. S. Dhesi, P. Bencok, N. B. Brookes, I. Marenne, P. Rudolf, N. Tagmatarchis, H. Shinohara, and T. J. S. Dennis, Phys. Rev. B **69**, 184421 (2004).
[31] Y. Teramura, A. Tanaka, B. T. Thole, and T. Jo, J. Phys. Soc. Jpn. **65**, 3056 (1996).
[32] F. Bondino, C. Cepek, N. Tagmatarchis, M. Prato, H. Shinohara, and A. Goldoni, J. Phys. Chem. B **110**, 7289 (2006).
[33] D. L. Cortie, J. D. Brown, S. Brück, T. Saerbeck, J. P. Evans, H. Fritzsche, X. L. Wang, J. E. Downes, and F. Klose, Phys. Rev. B **89**, 064424 (2014).